Distance-Dependent Fluorescence Quenching on Gold Nanoparticles Ensheathed with Layer-by-Layer Assembled Polyelectrolytes

ARTICLE *in* NANO LETTERS · APRIL 2006

Impact Factor: 13.59 · DOI: 10.1021/nl052441s · Source: PubMed

6 AUTHORS, INCLUDING:

Grégory F. Schneider
Leiden University
25 PUBLICATIONS **1,670** CITATIONS

SEE PROFILE

NANO LETTERS

2006
Vol. 6, No. 3
530−536

Distance-Dependent Fluorescence Quenching on Gold Nanoparticles Ensheathed with Layer-by-Layer Assembled Polyelectrolytes

Grégory Schneider and Gero Decher*

Institut Charles Sadron, CNRS UPR022, 6 rue Boussingault, F-67083 Strasbourg Cedex, France, and Université Louis Pasteur (ULP), 1 rue Blaise Pascal, F-67008 Strasbourg Cedex, France

Nicolas Nerambourg, Raïssa Praho, Martinus H. V. Werts,* and Mireille Blanchard-Desce

Synthèse et Electrosynthèse Organiques, CNRS UMR6510, Université de Rennes 1, Campus de Beaulieu, Bât. 10A, F-35042 Rennes Cedex, France

Received December 9, 2005; Revised Manuscript Received January 11, 2006

ABSTRACT

We report on the preparation, characterization, and photophysical study of new fluorescent core/shell nanoparticles fabricated by electrostatic layer-by-layer assembly. On the basis of gold cores with a diameter of 13 nm, these nanocolloids possess different fluorescently labeled polymer corona layers at various distances from the surface of the core metal using nonfluorescent polyelectrolytes as spacer layers. UV–visible spectroscopy and transmission electron microscopy confirm that the particle suspensions of fluorescently labeled core/shell nanoparticles are stable at all stages of their construction. Photophysical investigations reveal strongly distance-dependent fluorescence quenching in these particle systems. The contribution of the metal core to this quenching can be assesed precisely after the gentle dissolution of the gold cores by potassium cyanide. The photophysical measurements reveal clearly that the gold nanoparticles decrease the transition probability for radiative transitions.

Metal nanostructures can have interesting and potentially useful effects on the photoluminescence of nearby emitters. Molecular chromophores situated in the vicinity of isolated colloidal metal particles in suspension usually experience quenching of their fluorescence,[1−10] whereas photoluminescence may be enhanced in more complex structures that arise from the deposition of aggregated metal particles onto surfaces.[11−14] In the latter case, the enhanced luminescence appears to arise from certain "hot spots" where the metal is structured such that the local electromagnetic field is highly concentrated. An interesting challenge in this context would be to try and see if these "photonic hot spots" may be self-assembled in solution. For such an endeavor, it is important to know in detail the photophysical behavior of the more simple systems that may eventually constitute the building blocks for such assemblies.

In this letter, we describe the use of layer-by-layer (LBL) deposition[15−18] of oppositely charged polyelectrolytes onto 13-nm-diameter gold colloids to fabricate metal core-polymer shell capsules in which fluorescent organic dyes fluorescein and lissamine rhodamine B (in the following referred to as lissamine or LISS, Scheme 1) are situated at various distances from the gold core. LBL-coated gold nanoparticles have been reported before,[19,20] but this earlier work only describes LBL-shells of up to eight layers with unknown synthetic yields. However, the work in the present manuscript requires the assembly of 20 and more layers, including layers with functional groups, which requires robust coating conditions and a high stability of the nanoparticle dispersion like that reported previously by us.[21] The limpid and optically dilute suspensions of the dye-labeled core−shell particles can be studied readily by the methods of molecular fluorescence spectroscopy in solution. A useful property of the metal-containing core−shell particles is that the gold core can be dissolved gently by the addition of cyanide ions, which allows for a direct and precise comparison of the photophysical behavior of the fluorophores in the presence and absence of the metal nanocore. The photophysical investiga-

* Corresponding authors. E-mail: decher@ics.u-strasbg.fr; martinus.werts@univ-rennes1.fr.

10.1021/nl052441s CCC: $33.50
Published on Web 01/27/2006

Scheme 1. Layer-by-Layer Assembly for the Construction of Core−Shell Nanoparticles Containing Fluorescent Corona Layers[a]

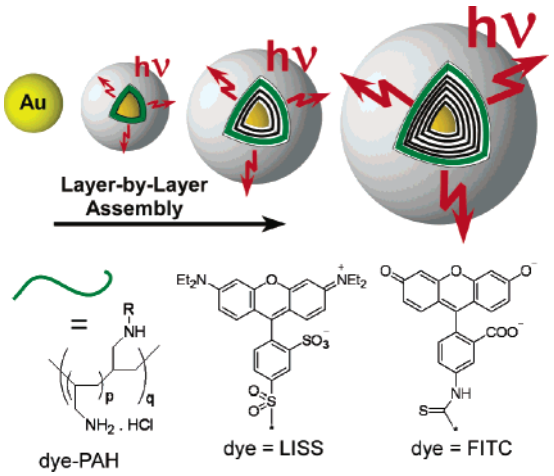

[a] The distance between the metal cores and the fluorescent layers is conveniently adjusted by varying the number of nonfluorescent layers (in black/white) between the gold nanoparticle core and the fluorescent layer (in green), thereby fine-tuning the photophysical properties of these nanodevices. The chemical structures of the fluorescently labeled poly(allylamine) and the dyes are shown in the bottom part.

tion of fluorophores positioned at well-defined distances near metal nanoparticles is not only of interest for nanoscale optics but especially also for the domain of functionalized metal colloids,[22,23] which may for example find applications in biomedical diagnostics,[24,25] where information is frequently conveyed by fluorescence.

Gold nanoparticles were synthesized using the reduction of tetrachloroauric acid by trisodium citrate.[26,27] Several primer layers of low molecular weight poly(allylamine hydrochloride) (PAH, $M_W = 15\,000$ g/mol) and poly(stryrene sulfonate) (PSS, $M_W = 13\,400$ g/mol) were adsorbed consecutively in a layer-by-layer fashion, to obtain Au nanoparticles coated with 2, 10, and 20 layers (Au(PAH/PSS)$_n$).[21] Fluorescein isothiocyanate (FITC) and lissamine rhodamine B sulfonyl chloride (LISS) were covalently attached to PAH to obtain PAH−FITC and PAH−LISS, respectively (see the Supporting Information). Only a small fraction (approximately 1%) of the available amino groups was labeled. PAH−FITC or PAH−LISS were adsorbed onto the Au(PAH/PSS)$_n$ core−shell particles, followed by the adsorption of a final PSS layer (see Scheme 1). After each of the deposition steps, the particles were washed thoroughly by successive centrifugation/resuspension cycles.

Transmission electron microscopy (TEM) investigations on Au(PAH/PSS)$_n$(PAH−FITC) revealed mean distances between the surface of the Au core and the fluorescent layer of about 1.5 ± 0.3 nm ($n = 1$), 4.0 ± 0.5 nm ($n = 5$), and 7.9 nm ± 0.7 nm ($n = 10$), respectively; for the case of Au(PAH/PSS)$_n$(PAH-LISS), the corresponding distances were 1.8 ± 0.3 nm ($n = 1$), 3.9 ± 0.5 ($n = 5$), and 7.7 ± 0.6 nm ($n = 10$), respectively. TEM micrographs of individual coated dye-labeled nanoparticles are shown at the right of Figure 1 for 1, 5, and 10 spacer pairs of PAH/PSS

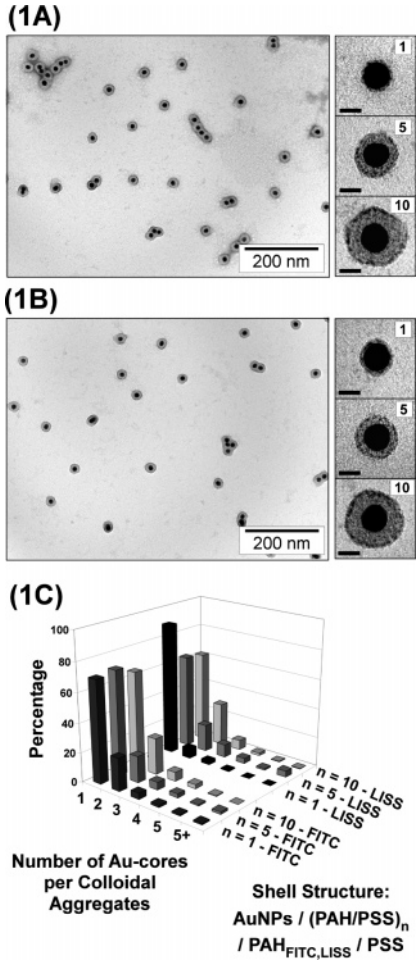

Figure 1. (A) Left: Transmission electron micrograph (TEM) overview on particles bearing 10 primer pairs of PAH/PSS layers and further coated with PAH−FITC, Au(PAH/PSS)$_{10}$(PAH−FITC). Right: TEM of LBL-coated individual gold nanoparticles ensheathed with $n = 1$, 5, and 10 pairs of PAH/PSS spacer layers, respectively, with a last layer of PAH−FITC, Au(PAH/PSS)$_n$-(PAH−FITC), before deposition of the terminating PSS layer. All samples were stained with uranyl acetate. (B) Left: TEM overview on lissamine-functionalized Au(PAH/PSS)$_{10}$(PAH-LISS). Right: TEM of LBL coated individual Au(PAH/PSS)$_n$(PAH-LISS) nanoparticles, with $n = 1$, 5, and 10. (C) Statistical evaluation of the aggregation state derived from TEM images of 2000 Au cores.

layers. The LBL-assembled shells were stained with uranyl acetate in order to enhance the contrast of the images. The left side of Figure 1 shows overviews of samples of such particles that are composed of a majority of single particles but also of a few aggregates with two or more Au cores. The statistical evaluation of the aggregation state derived from the TEM images is reported in the Figure 1C for 1, 5, and 10 primer pairs of layers with PAH−FITC and PAH−LISS. Because aggregation may take place during the preparation of the TEM grids, the statistics obtained through TEM measurements are to be considered as a "worst-case" representation of the distribution in the suspensions on which the photophysical measurements are done. In all suspensions, over 60% of the core−shell particles exist as isolated entities.

UV−visible absorption spectra taken during layer build-up (see the Supporting Information, Figure S1) indicate that the incorporation of fluorescent polyelectrolytes (PAH−FITC

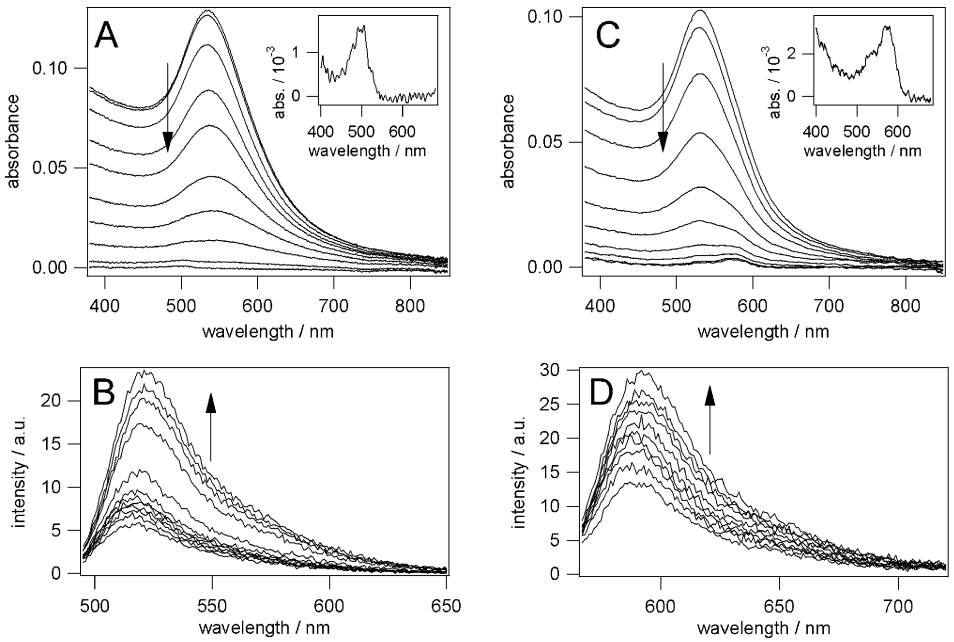

Figure 2. (A) Evolution in time of the absorption spectrum of a solution of $Au(PAH/PSS)_5(PAH-FITC/PSS)$ in 1 mM TRIS buffer upon addition of 1 mM KCN. The first spectrum was taken before addition of KCN. The complete disappearance of the gold nanocore takes approximately 4 h. The inset shows a close-up of the residual dye absorbance after 1 night. (B) Corresponding emission spectra ($\lambda_{exc} = 490$ nm). (C) Evolution of the absorption spectrum of $Au(PAH/PSS)_5(PAH-LISS/PSS)$ in water upon addition of 1 mM KCN. (D) Emission spectra corresponding to C ($\lambda_{exc} = 563$ nm).

and PAH−LISS) does not significantly perturb layer growth or the aggregation state of the particles as illustrated by the absence of spectral changes due to aggregation even when only a few polymer layers are adsorbed (case $n = 1$). This is explicitly stated here because this is the first report in which functionalized polymers (in this case carrying fluorophores) are used in the deposition sequence. Additionally, one can safely continue to deposit at least one layer of PSS on top of the fluorescent layer that generates an increase of the PSS absorption band at 225 nm. After several layers ($n > 5$), the surface plasmon (SP) resonance appears to reach a fixed intensity and position at 534 nm in the case of PAH−FITC and near 533 nm for PAH−LISS. This dependence of the position and the intensity of the SP band on the number of deposited layers is due to dielectric screening of the SP by the adsorbed polymers.

Because of the low level of dye labeling of the outer polymer layer, the UV−visible absorption spectra of the core−shell particles (Figure 2A and C) do not show any clearly distinguishable dye-related absorption bands, being completely dominated by the intense SP absorption of the gold nanocore. The presence of the dyes, however, becomes evident through the observation of their typical emission spectra under excitation at their characteristic absorption wavelengths (Figure 2B and D). Fluorescence excitation spectra (not shown) confirm their identity because they reveal the typical absorption profile of each dye.

Attempts to isolate the absorption bands of the dyes through numerical subtraction of the absorption spectra of unlabeled particles did not yield unambiguous and conclusive results. However, the fact that metallic gold is used as the nanoparticle core allows for the removal of the surface plasmon band by dissolving the gold with the help of cyanide ions. This is an elegant procedure, which, however, requires highly stable particle suspensions and low cyanide concentrations in order to avoid particle aggregation caused by electrostatic screening. In previous work on this type of core−shell material, the removal of the gold core was shown to result in empty nanospheres.[19,21] In the present experiments, the dissolution of gold is started by adding a small volume (typically 20 μl) of a stock solution (10 g L^{-1}) of KCN in water to the particle suspension contained in the fluorescence cuvette to bring the concentration of KCN in the cuvette to 1 mM. The evolution of the UV−visible absorption and fluorescence emission spectra was followed in time.

As shown in Figure 2A and C, dissolution of the gold core by cyanide leads to a gradual disappearance of the gold surface plasmon absorption. After completion of this process, a weak absorption band remains, which corresponds to light absorption by the dye, the fluorescent dye remaining chemically unchanged after this mild dissolution of the core. The dissolution of the metallic cores is accompanied by a strong increase of the observed fluorescence (Figure 2B and D). All fluorescence spectra have been fully corrected, including a correction for inner-filter effects (see the Supporting Information). Thus, they represent the intrinsic emission spectra and intensities of the dye-labeled capsules without any contibutions from experimental factors such as wavelength-dependence of the detector response or reabsorption of emitted light by the solution itself.

The etching reaction results in the formation of "lost template" fluorescent nanospheres independent of the number of primer layers, as shown in Figure 3. The dark spot observed in the inside of the particles may be due to the presence of uranyl acetate in the empty core of the sphere.

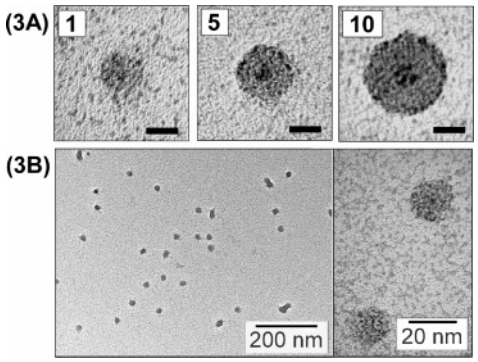

Figure 3. (A) Transmission electron micrographs (TEM) of uranyl-stained LBL nanospheres consisting of 2, 10, and 20 layers of alternating PAH and PSS ((PAH/PSS)$_n$(PAH−FITC/PSS) with n = 1, 5, and 10) after complete gold core dissolution by an etching reaction with potassium cyanide. The bar corresponds to 10 nm. (B) Overview TEM micrograph of the empty nanospheres after dissolution of the gold core by cyanide and staining with uranyl acetate (left). Enlarged picture on two individual "lost template" nanospheres (right).

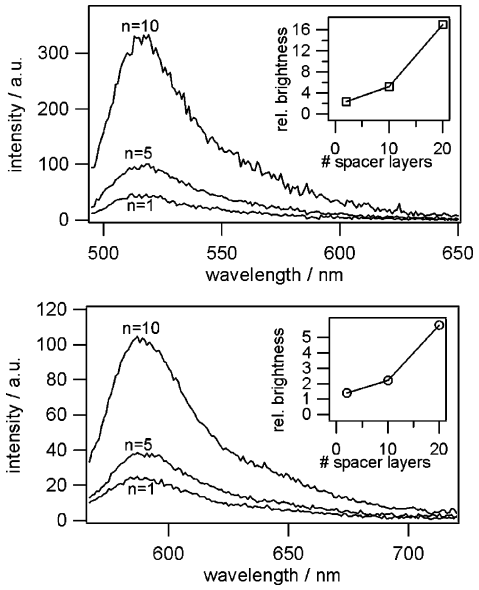

Figure 4. Fully corrected emission spectra of core−shell nanoparticles of structure Au(PAH/PSS)$_n$(PAH−FITC/PSS) (top, λ_{exc} = 490 nm) and Au(PAH/PSS)$_n$(PAH-LISS/PSS) (bottom, λ_{exc} = 563 nm) in aqueous suspension. Spectra have been scaled to equal concentrations of dye, determined through the residual UV/vis absorption band after complete etching of the gold core by 1 mM KCN. Thus, their areas represent the relative brightness (proportional to the product of extinction coefficient and fluorescence quantum yield) of the dyes near the metal core.

This spot is not visible when particles are not stained and may be related to the hollowness of these nanospheres. The overview TEM micrograph shown in Figure 3B shows little to no changes in the aggregation state of the nanoparticles with a majority of single particles and few doubles or triples like those reported in Figure 1.

The dye absorption bands remaining after dissolution of the cores enable a reliable determination of the relative dye concentration in each sample, irrespective of fluctuations in polymer layer deposition efficiencies, which may introduce batch-to-batch variations in the level of dye loading of the core−shell particles (UV−visible spectrometry might actually be used to study these fluctuations). The information about the dye concentration obtained after dissolution of the gold core was used to scale the fluorescence emission spectra of the initial metal-core polymer-shell capsules. The scaled spectra are shown in Figure 4. The areas under the spectra represent the relative brightness of dye fluorescence for each type of core−shell capsule. The relative brightness is proportional to the product, $\epsilon\Phi$, of the extinction coefficient and the fluorescence quantum yield of the incorporated dye. It is expressed on a "per molecule" (or "per molar") basis and conveys how the fluorescent behavior of an average dye molecule changes as it is positioned nearer and nearer to the gold nanocore. We note that in this context the number of fluorescent dye molecules per particle is not important. For completeness, we estimated these numbers on the basis of the UV−visible absorption data. The number of fluorescein dye molecules per core−shell particle Au(PAH/PSS)$_n$-(PAH−FITC/PSS) are estimated to be 60 (n = 1), 62 (n = 5), and 43 (n = 10). The numbers for Au(PAH/PSS)$_n$(PAH−LISS/PSS) are 68 (n = 1), 85 (n = 5), and 74 (n = 10). This justifies that approximately 40−60 PAH chains adsorb per nanoparticle at these stages of deposition.

There is a clear rise in relative brightness as the number of spacer layers separating the dye and the metal core increases, which confirms the distance dependence of the fluorescence quenching. Instead of considering the fluorescence quantum yield, Φ, alone, it is more appropriate to discuss the photoluminescence spectra of these metal-containing capsules in terms of brightness ($\epsilon\Phi$). We will see below that the fluorescence quenching is partly due to a decrease in the probability of spontaneous emission, in which case there is likely to be an effect on the transition probability of absorption as well, potentially leading to a change in extinction coefficient.[28,29] Thus, changes in observed fluorescence intensity may depend on both changes in light absorption and emission probabilities.

In the case of the empty nanospheres obtained upon cyanide-induced disolution of the gold core, we have direct access to the absorbance spectrum, which enables us to measure the fluorescence quantum yields of the dyes in these empty polymer capsules using quinine bisulfate in 0.5 M H_2SO_4 (Φ = 0.546) as a reference. The quantum yield data for the empty capsules (Table 1) suggest that the polymer matrix also has an effect on the fluorescence of the incorporated dye. Compared to the free dyes, the quantum yields of the polymer-bound dyes and the dyes incorporated in the shell of empty capsules are diminished. This is not unexpected; it is known that fluorescence quenching can occur through electron transfer from nearby free amino groups. Variations in the local pH, which may affect fluorescein and are known to exist in LBL structures,[30] are unlikely to play a role because the suspensions were buffered at pH 8.3, a pH significantly above the first pK_a of the fluorescein chromophore, 6.4. This is substantiated by the UV−visible spectra of the empty capsules, which show that the fluorescein chromophore is in its dianion form. The presence of less fluorescent, protonated forms of fluorescein

Table 1. Effect of the Polymer Matrix on Dye Fluorescence[a]

	dye = FITC	dye = LISS
free dye in solution	1.0[b]	0.37
PAH-bound dye in solution	0.30	0.41
$(PAH/PSS)_1(PAH-dye/PSS)$	0.20	0.07
$(PAH/PSS)_5(PAH-dye/PSS)$	0.22	0.05
$(PAH/PSS)_{10}(PAH-dye/PSS)$	0.32	0.10

[a] Absolute fluorescence quantum yields (Φ) of the free dyes in solution, the polymer bound dyes in solution, and the dyes incorporated in the empty polymer capsules, after dissolution of the gold core by 1 mM KCN. The estimated error in the quantum yield values is ±15% for the free dye and the polymer. It amounts to ±30% for the capsules because of the weakness of UV/vis absorption of the solutions. The fluorescein (FITC) samples were measured in 1 mM TRIS + 1 mM KCN (pH 8.3); the lissamine (LISS) samples were measured in 1 mM KCN. [b] Free fluorescein (not FITC) in solution.

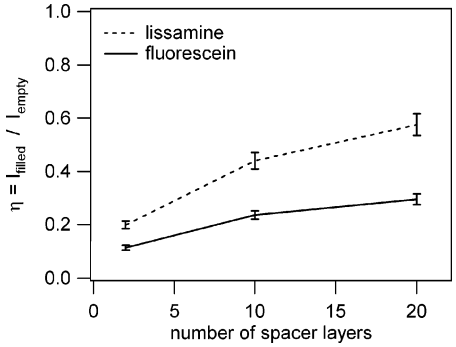

Figure 5. Fluorescence intensity of core−shell $Au(PAH/PSS)_n$-(PAH-dye/PSS) nanoparticles relative to the intensity of the corresponding empty nanocapsules after removal of the gold core as a function of the number of polymer layers separating the dye-doped polymer layer from the core of the capsules.

would show up in the absorption spectra by the appearance of an additional absorption band at shorter wavelengths. Compared to fluorescein, lissamine appears to be particularly affected by the incorporation in the layer-by-layer polymer capsules. It may be that this dye is more sensitive to electron transfer quenching by amino groups than fluorescein. The polymers inside the layer-by-layer structure are probably more compact than the free polymers in solution, leading to a larger proximity of quenching amino groups.

The effect of the metal nanocore on the fluorescence of the dyes can be quantified by evaluating the ratio of the areas under the fluorescence spectra before (I_{full}) and after (I_{empty}) the core dissolution: $\eta = I_{full}/I_{empty}$. Because these two fluorescence intensity measurements are done on the same sample, the concentration of the dye is rigorously the same (the cyanide only attacks the gold leaving the dyes and the polymer shells intact, as evidenced by optical spectroscopy, Figure 2, and TEM, Figure 3). Thus, the ratio, η, can be measured with good certainty. Moreover, the dyes are kept in the same polymer environment, the only difference being the presence or absence of the metal core, and η reflects the effect of the gold nanocore alone. This is important because it allows us to study the effect of the metal core alone, canceling out any effects of the polymer matrix. Figure 5 contains a plot of ratio η versus the number of spacer layers separating the dye and the core. It shows that the metal core-induced fluorescence quenching becomes significantly stronger as the dye approaches the metal.

Table 2. Variations of the Fluorescence Intensities and Lifetimes upon Removal of the Gold Nanocore from Fluorescein-Labeled $Au(PAH/PSS)_n(PAH-FITC/PSS)$ Capsules[a]

	η	τ_{full}/ns	τ_{empty}/ns	α
$n = 1$	0.11 ± 0.01	3.2 ± 0.2	3.3 ± 0.2	0.34 ± 0.02
$n = 5$	0.24 ± 0.02	3.3 ± 0.1	3.7 ± 0.1	0.52 ± 0.02
$n = 10$	0.29 ± 0.02	3.1 ± 0.1	4.0 ± 0.1	0.61 ± 0.02

[a] $\eta = I_{full}/I_{empty}$. τ_{full} and τ_{empty} represent the fluorescence lifetimes of the full core−shell particles and empty capsules, respectively, measured by TCSPC. α is the factor by which the radiative rate of the chromophore is changed in the presence of the golden nanocore, $\alpha^2 = \eta\tau_{empty}/\tau_{full}$.

Insight of the origin of the quenching is obtained by combining the steady-state value, η, with fluorescence lifetime data. Fluorescence decay traces were obtained for $Au(PAH/PSS)_n(PAH-FITC/PSS)$ and the corresponding empty capsules using time-correlated single photon counting (TCSPC) under excitation with a nanosecond flash lamp. Unfortunately, TCSPC measurements for the lissamine particles proved to be impossible using our current setup because of the absence of sufficient excitation intensity at the wavelength required. The fluorescein particles already required long aquisition times. For all samples, a mono-exponential fluorescence decay was observed (see the Supporting Information, Figure S2). The fluorescence lifetimes do not change drastically on going from a particle containing a metal core to the corresponding empty capsule, even when the overall fluorescence intensity is greatly affected (Table 2).

The observed fluorescence decay time, τ, is determined by the radiative rate constant, k_r, and its nonradiative counterpart, k_{nr}: $\tau = (k_r + k_{nr})^{-1}$. It is related to the fluorescence quantum yield through

$$\Phi = k_r\tau \tag{1}$$

Often, molecular fluorescence is quenched by nonradiative processes that augment k_{nr} but do not change k_r. As a result, changes in fluorescence quantum yield will be accompanied by a proportional change of the observed decay time. In the case of the $Au(PAH/PSS)_n(PAH-FITC/PSS)$ particles, there is no such proportionality, suggesting that there the metal core induces a change in k_r. The ratio, η, of the fluorescence intensity of a solution of gold-core-containing particles and that of the same solution after complete removal of the gold nanocores is equal to the ratio of the brightnesses, $\epsilon\Phi$, of the full and empty capsules where ϵ is the molar extinction coefficient.

$$\eta = \frac{I_{full}}{I_{empty}} = \frac{(\epsilon\Phi)_{full}}{(\epsilon\Phi)_{empty}} = \frac{\epsilon' k_r' \tau_{full}}{\epsilon\, k_r \tau_{empty}} \tag{2}$$

where ϵ' and k_r' are the extinction coefficient and the radiative rate constant for the gold-containing capsules. The change in radiative rate induced by the gold nanocore may be

represented by an empirical factor, α, such that $k_r' = \alpha k_r$. A change in this spontaneous emission transition probability might be accompanied by a change in the probability for absorption. Here we tentatively assume that $\epsilon' = \alpha\epsilon$,[28,29] although we are aware that the Einstein relation between absorption and spontaneous emission is defined for isotropic media, which is not the case here. Theoretical models describing light emitters and absorbers near a metal particle more explicitly may be applicable.[31] Assuming that the Einstein relation holds, the factor α can be obtained from our experimental data through

$$\alpha^2 = \eta \frac{\tau_{\text{empty}}}{\tau_{\text{full}}} \tag{3}$$

All three parameters in eq 3 (η, τ_{empty}, and τ_{full}) can be measured with relative ease and reliability on the same solution, before and after exposure to 1 mM KCN. In a certain sense, the sample serves as its own reference. The values of α for different fluorescein−gold nanocore separations are in Table 2. As the fluorescein dye approaches the core surface, its radiative transition probabilities appear to drop to 34% of its original value at a distance of 1.5 nm. The observed reduction in radiative rate may be reflected in changes of the extinction coefficient,[28,29] but reliable determination of the dye absorption bands in the presence of the metal core has not been possible here because of the low dye-labeling levels applied. The effect might be observed in particles having higher dye loadings, such that the absorption band of the dyes may be more readily distinguished from the surface plasmon absorption band. Profound changes in the absorption spectrum of J aggregates of a cyanine dye adsorbed directly onto the surface of silver and gold nanoparticles have been observed recently.[32]

Studies on the direct effect of the metal particle core on molecular light absorption may clarify whether the transition probabilities for absorption and emission are affected in the same way. If this is not the case, then the α^2 term in eq 3 needs to be replaced by the product ($\alpha_{abs}\alpha_{em}$) of the changes in absorption and spontaneous emission probabilities. Direct access to the absorption spectrum of the dyes in the presence of the metal core may also shed more clarity onto the apparent discrepancy between the fact that the spectral position of the surface plasmon practically ceases to shift after deposition of 10 layers (5 pairs) of polymers, whereas the reduction of photoluminescence by the particle core occurs for even twice that distance. It may be that the presence of the (very weak) dye absorption partially obscures further shifts of the SP band. In previous work,[21] the SP band of gold nanoparticles coated using unlabeled PAH and PSS continues to shift slightly even after the deposition of 20 polymer layers.

In conclusion, the gold nanocore quenches the fluorescence of the fluorescein and lissamine dyes situated in the outer polymer layers of the core−shell nanoparticles. Even with 20 spacer layers (i.e., 10 pairs of PAH/PSS, corresponding to a dye-nanocore distance of 8 nm), this quenching is significant. Nonetheless, the fluorescence of the core−shell particles remains sufficiently bright for potential applications as diagnostic or sensing devices. Combining the measured relative brightness and observed fluorescence decay times of the set of fluorescein-containing core−shell nanoparticles, we find clear indications that an important part of the fluorescence quenching is due to a reduction of the radiative rate, which is in agreement with very recent findings by Dulkeith et al.[10] Quantitave experimental examples of the effect of isolated metal nanoparticles on the radiative rate of nearby photoluminescent emitters are scarce. In this Letter, the distance between dye and metal core is controlled reliably through LBL assembly, and the fluorescence measurements give a direct access to the effect of the metal core on the radiative rates.

The layer-by-layer method is, in principle, applicable to other core materials, according to classical rules of colloidal chemistry.[33−35] It may thus be possible to change the shape, size, and composition of the metal core. LBL deposition enables precise control of the distance separating the photoactive units and the metal core and provides the flexibility for the facile integration of different chromophores and other functionalities. The "lost template" photoactive nanospheres obtained after dissolution of the gold core constitute in themselves interesting objects that can form the basis of multifunctional fluorescent sensors or perhaps even photocontrollable delivery agents. From a more fundamental point of view, the physicochemical behavior (e.g., molecule and ion permeability etc.) of these objects may be an interesting subject of further studies.

Acknowledgment. Financial support from Rennes Métropole, Université de Rennes 1 (BQR), and the Ministère de l'Education Nationale, de la Recherche et de la Technologie is gratefully acknowledged. Annette Thierry and Marc Schmutz are also acknowledged for their invaluable help and support in transmission electron microscopy.

Supporting Information Available: Preparation of the materials and details of spectroscopic measurements. This material is available free of charge via the Internet at http://pubs.acs.org.

References

(1) Aguila, A.; Murray, R. W. *Langmuir* **2000**, *16*, 5949−5954.
(2) Hu, J.; Zhang, J.; Liu, F.; Kittredge, K.; Whitesell, J. K.; Fox, M. A. *J. Am. Chem. Soc.* **2001**, *123*, 1464−1470.
(3) Ipe, B. I.; Thomas, K. G.; Barazzouk, S.; Hotchandani, S.; Kamat, P. V. *J. Phys. Chem. B* **2002**, *106*, 18−21.
(4) Huang, T.; Murray, R. W. *Langmuir* **2002**, *18*, 7077−7081.
(5) Gu, T.; Whitesell, J. K.; Fox, M. A. *Chem. Mater.* **2003**, *15*, 1358−1366.
(6) Montalti, M.; Prodi, L.; Zaccheroni, N.; Battistini, G. *Langmuir* **2004**, *20*, 7884−7886.
(7) Werts, M. H. V.; Zaim, H.; Blanchard-Desce, M. *Photochem. Photobiol. Sci.* **2004**, *3*, 29−32.
(8) Gueroui, Z.; Libchaber, A. *Phys. Rev. Lett.* **2004**, *93*, 166108.
(9) Ghosh, S. K.; Pal, A.; Kundu, S.; Nath, S.; Pal, T. *Chem. Phys. Lett.* **2004**, *395*, 366−375.
(10) Dulkeith, E.; Ringler, M.; Klar, T. A.; Feldmann, J.; Javier, A. M.; Parak, W. J. *Nano Lett.* **2005**, *5*, 585.
(11) Kummerlen, J.; Leitner, A.; Brunner, H.; Aussenegg, F. R.; Wokaun, A. *Mol. Phys.* **1993**, *80*, 1031−1046.
(12) Gryczynski, I.; Malicka, J.; Holder, E.; DiCesare, N.; Lakowicz, J. R. *Chem. Phys. Lett.* **2003**, *372*, 409−414.

(13) Wenseleers, W.; Stellacci, F.; Meyer-Friedrichsen, T.; Mangel, T.; Bauer, C. A.; Pond, S. J. K.; Marder, S. R.; Perry, J. W. *J. Phys. Chem. B* **2002**, *106*, 6853−6863.
(14) Pan, S.; Rothberg, L. J. *J. Am. Chem. Soc.* **2005**, *127*, 6087.
(15) Decher, G.; Hong, J.-D.; Schmitt, J. *Thin Solid Films* **1992**, *210*−*211*, 831−835.
(16) Decher, G. In *Comprehensive Supramolecular Chemistry: Templating, Self-Assembly and Self-Organization*; Sauvage, J.-P.; Hosseini, M. W., Eds.; Pergamon Press: Oxford, U.K., 1996; Vol. 9, pp 507−528.
(17) Decher, G. *Science* **1997**, *277*, 1232−1237.
(18) Decher, G.; Schlenoff, J. B. *Multilayer Thin Films: Sequential Assembly of Nanocomposite Materials*; Wiley-VCH: Weinheim, Germany, 2003.
(19) Gittins, D. I.; Caruso, F. *Adv. Mater.* **2000**, *12*, 1947−1949.
(20) Gittins, D. I.; Caruso, F. *J. Phys. Chem. B* **2001**, *105*, 6846−6852.
(21) Schneider, G.; Decher, G. *Nano Lett.* **2004**, *4*, 1833−1839.
(22) Daniel, M.-C.; Astruc, D. *Chem. Rev.* **2004**, *104*, 293−346.
(23) Katz, E.; Willner, I. *Angew. Chem., Int. Ed.* **2004**, *43*, 6042−6108.
(24) Demers, L. M.; Mirkin, C. A.; Mucic, R. C.; Reynolds, R. A., III; Letsinger, R. L.; Elghanian, R.; Viswanadham, G. *Anal. Chem.* **2000**, *72*, 5535−5541.
(25) Hamad-Schifferli, K.; Schwartz, J. J.; Santos, A. T.; Zhang, S.; Jacobson, J. M. *Nature* **2002**, *415*, 152−155.
(26) Turkevich, J.; Stevenson, P. C.; Hillier, J. *Discuss. Faraday Soc.* **1951**, *11*, 55−75.
(27) Frens, G. *Nature (London), Phys. Sci.* **1973**, *241*, 20−22.
(28) Strickler, S. J.; Berg, R. A. *J. Chem. Phys.* **1962**, *37*, 814−822.
(29) Einstein, A. *Physik. Z.* **1917**, *18*, 121−128.
(30) von Klitzing, R.; Möhwald, H. *Langmuir* **1995**, *11*, 3554−3559.
(31) Gersten, J.; Nitzan, A. *J. Chem. Phys.* **1981**, *75*, 1139−1152.
(32) Wiederrecht, G. P.; Wurtz, G. A.; Hranisavljevic, J. *Nano Lett.* **2004**, *4*, 2121−2125.
(33) Vincent, B. *Adv. Colloid Interface Sci.* **1974**, *4*, 193−277.
(34) Heller, W.; Pugh, T. L. *J. Polym. Sci.* **1960**, *47*, 203-217.
(35) Pugh, T. L.; Heller, W. *J. Polym. Sci.* **1960**, *47*, 219−227.

NL052441S